GRIFFITH UNIVERSITY

# Miniaturized optoelectronic tweezers controlled by GaN micro-pixel light emitting diode arrays


## Author

Zarowna-Dabrowska, Alicja, Neale, Steven L., Massoubre, David, McKendry, Jonathan, Rae, Bruce R., Henderson, Robert K., Rose, Mervyn J., Yin, Huabing, Cooper, Jonathan M., Gu, Erdan, Dawson, Martin D.



## Published

2011

## Journal Title

Optics Express

## DOI

10.1364/OE.19.002720



## Rights statement

© 2011 OSA. This paper was published in Optics Express and is made available as an electronic reprint with the permission of OSA. The paper can be found at the following URL on the OSA website: http://dx.doi.org/10.1364/OE.19.002720. Systematic or multiple reproduction or distribution to multiple locations via electronic or other means is prohibited and is subject to penalties under law.

## Downloaded from

http://hdl.handle.net/10072/52462

## Griffith Research Online

https://research-repository.griffith.edu.au

# Characterization of miniaturized optoelectronic tweezers controlled by GaN micro-pixel light emitting diode arrays

**Alicja Zarowna-Dabrowska [1,2], Steven L. Neale [2*], David Massoubre [1], Jonathan McKendry [1], Bruce R. Rae [3], Robert K. Henderson [3], Mervyn J. Rose [4], Huabing Yin [2], Jonathan M. Cooper [2] Erdan Gu [1*], and Martin D. Dawson [1]**

*1 Institute of Photonics, University of Strathclyde, Glasgow, UK*
*2 School of Engineering, University of Glasgow, UK*
*3 Institute for Integrated Micro and Nano Systems, Joint Research Institute for Integrated Systems, The School of Engineering,University of Edinburgh, UK*
*4 Electronic Engineering and Physics, University of Dundee,UK*
*[*]s.neale@elec.gla.ac.uk and erdan.gu@strath.ac.uk*

**Abstract:** CMOS-controlled GaN micro-pixel light emitting diode arrays have been used to create reconfigurable light-patterned electrodes in a miniaturized optoelectronic tweezers (OET) device. We present this micro-system's capabilities for manipulating micro-particles including beads and cells and consider the implications of the approach for multifunctional OET trapping and measurement in an integrated format.

©2010 Optical Society of America

**OCIS codes:** (000.0000) General; (000.2700) General science.

## References and links

1. Xie, H., D.S. Haliyo, and S. Regnier, *A versatile atomic force microscope for three-dimensional nanomanipulation and nanoassembly.* Nanotechnology, 2009. **20**(21): p. 215301.
2. Stevenson, D.J., F. Gunn-Moore, and K. Dholakia, *Light forces the pace: optical manipulation for biophotonics.* Journal of Biomedical Optics. **15**(4). Year?
3. Pethig, R., *Review Article-Dielectrophoresis: Status of the theory, technology, and applications.* Biomicrofluidics. **4**(2).Year?
4. Vieira, G., et al., *Magnetic Wire Traps and Programmable Manipulation of Biological Cells.* Physical Review Letters, 2009. **103**(12).
5. Yamakoshi, Y., et al., *Yeast cell trapping in ultrasonic wave field using ultrasonic contrast agent.* Japanese Journal of Applied Physics Part 1-Regular Papers Brief Communications & Review Papers, 2006. **45**(5B): p. 4712-4717.
6. Chiou, P.Y., A.T. Ohta, and M.C. Wu, *Massively parallel manipulation of single cells and microparticles using optical images.* Nature, 2005. **436**(7049): p. 370-372.
7. Neale, S.L., et al., *The resolution of optical traps created by light induced dielectrophoresis (LIDEP).* Optics Express, 2007. **15**(20): p. 12619-12626.
8. Hwang, H., et al., *Interactive manipulation of blood cells using a lens-integrated liquid crystal display based optoelectronic tweezers system.* Electrophoresis, 2008. **29**(6): p. 1203-1212.
9. Jamshidi, A., *Optoelectronic Manipulation, Assembly, and Patterning of Nanoparticles*, in *Electrical Engineering and Computer Sciences*. 2009, University of California: Berkeley. p. 108.
10. Rae, B.R., et al., *A CMOS Time-Resolved Fluorescence Lifetime Analysis Micro-System.* Sensors, 2009. **9**(11): p. 9255-9274.
11. Gong, Z., et al., *Size-dependent light output, spectral shift, and self-heating of 400 nm InGaN light-emitting diodes.* Journal of Applied Physics, 2010. **107**(1).
12. McKendry, J., et al., *High speed visible light communications using individual pixels in a micro light-emitting diode array.* IEEE Photonics Technology Letters, 2010.
13. Street, R.A., *Technology and Applications of Amorphous Silicon*. Springer series in materials science. Vol. 37. 2000, New York: Springer. 417.
14. Kamei, T., et al., *Integrated hydrogenated amorphous Si photodiode detector for microfluidic bioanalytical devices.* Analytical Chemistry, 2003. **75**(20): p. 5300-5305.

15. Valley, J.K., et al., *Operational regimes and physics present in optoelectronic tweezers.* Journal of Microelectromechanical Systems, 2008. **17**(2): p. 342-350.

## 1. Introduction

The ability to manipulate micro-sized objects is essential for numerous cell biology experiments, for example observing cell interactions with other cells or their environment, or in cell sorting. There are many competing micromanipulation techniques being actively researched, including mechanical manipulation using AFM tips [1], optical tweezers [2], dielectrophoresis [3], magnetic traps [4] and acoustic traps [5]. Each technique has distinct advantages and disadvantages, with some offering higher forces whilst others offer more precise particle manipulation. A further, recently developed technique, Optoelectronic Tweezers (OET), uses a light patterned photoconductor to provide real time control over the positioning of electric fields. The OET device uses a photoconductive thin film electrode which is illuminated by a light pattern to create a similar pattern in the film's local conductivity. This creates non-uniform electric fields in liquid interfacing between the photoconductive electrode and a counter electrode. When a neutral particle is submerged into a non-uniform electric field the particle polarizes, a potential is created outside the particle and a dipole moment is induced. This effect is named dielectrophoresis (DEP) [3]. The DEP force can then be used to trap and move particles.

OET has advantages over traditional dielectrophoresis as the field can be repositioned and more particles can be manipulated individually and in parallel than with AFM, magnetic tweezers or optical tweezers [6]. The OET traps have been compared to optical traps and have found to be 470 times stiffer for a similar light intensity [7]. In addition, the optical properties of the particles do not constrain the manipulation. Disadvantages of OET are that it is a 2D force and the trapping is not as strong as with an AFM tip or with magnetic traps. There are also limitations on the liquids that the particles can be suspended in, with the liquid conductivity having to be within a certain range controlled by the conductivity of the photoconductor. The light pattern that creates the virtual electrode in an OET device has been created to date by either using a Digital Micro-mirror Device (DMD) [6] or using an LCD display [8]. However, these DMD and LCD devices are quite bulky, and have limited prospects for integration and multi-functional embodiments. In this work, we used CMOS controlled gallium nitride micro-pixel light emitting diode arrays (micro-LEDs) to create the light patterns. We demonstrate the capabilities of the resulting miniaturized OET device in particle manipulation.

## 2. OET device structure and working principle

A typical OET device [9] is composed of two electrodes made of ITO coated borosilicate glass slides. A conductive liquid is placed between them (fig.1a). Both electrodes are connected to a function generator and the bottom electrode is covered with a layer of the photoconductive material, where here we have used amorphous silicon (a-Si).In the dark, the impedance of the photoconductive layer is higher than the impedance of the liquid between the electrodes and almost all the voltage is dropped across the photoconductive layer (fig.1a). Under illumination, the impedance of the photoconductor drops dramatically and the voltage is transferred into the liquid surrounding the illuminated area (fig.1b). Under illumination, a non-uniform electric field is generated between two electrodes.

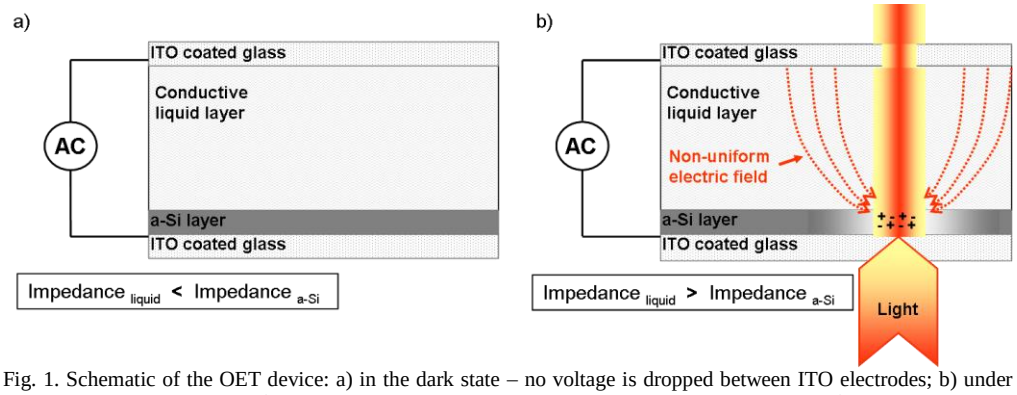


Fig. 1. Schematic of the OET device: a) in the dark state – no voltage is dropped between ITO electrodes; b) under illumination, the impedance of the photoconductive layer, a-Si, has dropped, the voltage is transferred into the liquid in the proximity of the illuminated area and a non-uniform electric field is generated between electrodes.

This non-uniform field creates a DEP force on neutral particles. The magnitude and direction of the force are determined by the relative permittivity of the particle and the liquid it is suspended in. Particles with high permittivity relative to the medium experience a force towards the high electric field region, i.e. positive DEP, while particles with lower permittivity experience a force away from the high field region, i.e. negative DEP (fig.2a). The DEP force is proportional to the electric field gradient, so is strongest, and dominates the particles' motion, at the edges of the illuminated area.

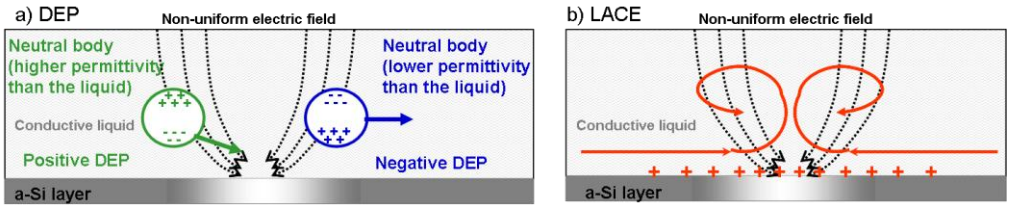


Fig. 2. Schematics of a) the dielectrophoresis (DEP) forces generated in the OET devices and the resultant particle movement and b) Light-induced AC electro-osmosis (LACE).and induced liquid movement.

In addition, when a low frequency AC bias is applied, a second force is experienced by ions at the liquid/solid interface. Small quantities of ions are suspended in the liquid and they have tendency to distribute near to the opposite charges appearing at the solid surface creating a double layer of ions. These ions feel a force due to the electric field, which is stronger at the illuminated region of the device attracting the positive ions in the liquid. The movement of the ions drags the bulk of the fluid with them. This phenomenon is named light-induced AC electro-osmosis (LACE) [9]. This liquid movement towards the illuminated area close to the surface, and away from the illuminated area above it, creates vortices (fig. 2b). This phenomenon is responsible for particles and liquid movement over relatively large distances (few millimeters from the illuminated area).

## 3. Miniaturised OET design and structure

### 3.1. Advantages of CMOS-controlled micro-LEDs

The OET device relies on the light pattern created inside the sample chamber. So far, the light pattern inside the OET device has been produced by bulky light sources: lasers, laser diodes, lamps, projected onto a digital micro-mirror device or a video-projector, and then the light has been coupled into the sample chamber with microscope lenses. The whole set up then takes up significant space on an optical table. By using CMOS controlled micro-LEDs we have miniaturized the illumination part dramatically.

Our CMOS-controlled micro-LEDs have 'micro-disk' pixels of ten to a few tens of microns in diameter, producing a light pattern with precise spatial control [10] directly from the light source rather than by using a spatial light modulator. This facilitates integration, offers independent pixel control and the possibility of switching modes of operation of the device (e.g. CW to sub-nanosecond pulsing [10] which can be used for combined manipulation and time-resolved fluorescence analysis). The micro-LED chips, each consisting of 8 x 8 arrays of micro-pixels flip-chip bump bonded to a CMOS control backplane, were fabricated with different emission wavelengths, specifically 450nm and 520nm, with different pixel sizes [10]. In this arrangement, light is extracted through the polished sapphire substrate. The typical turn-on voltage, drive current and power output of these LED micro-pixels depends on semiconductor wafer characteristics and pixel size [11]. We have used devices with pixel diameters from 14µm to 84µm (in 8 steps of 10µm) all on a center-to-center pitch of 200µm. A typical turn-on voltage for the 450nm devices is 3.0V and they can produce an output power up to 4.5mW per pixel (as measured for an 84µm pixel at a drive current of 140mA) [12]. The 520nm micro-LEDs have a typical turn-on voltage of 4.2V and an average output power of 300µW at 21mA for a 74µm pixel size. The micro-pixellated light source is powered and easily controlled by a computer through a USB connection.

### 3.2. Integration of the OET with micro-LEDs

#### 3.2.1. Adopted geometry

For a tweezing application the observation of the manipulated sample is very important. Unfavorably, the packaged micro-LED arrays are not transparent. Consequently, to create an integrated OET device, the micro-LEDs have been placed underneath the a-Si allowing observation of the sample chamber from the top of the OET device. Figure 3a) shows the arrangement used. In addition, a low-cost lens, 6 mm diameter and of NA 0.55 (Geltech™, ThorLabs) has been fixed on the top of micro-LEDs to focus their light onto the a-Si surface, as shown in figure 3b). The micro-LED light transmitted through the sapphire substrate in the 'flip-chip' device geometry used here diverges too much to be coupled directly to the OET device – the light pattern created without the lens and its gradient was too low to generate substantial, non-uniform electric fields which would create a force to move the particles.

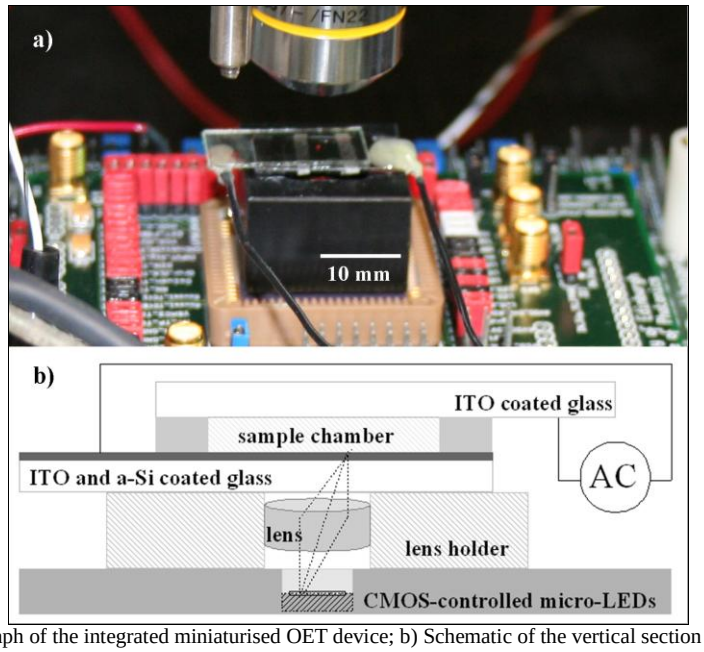

Fig. 3. a) Photograph of the integrated miniaturised OET device; b) Schematic of the vertical section of the device.

3.2.2. Wavelength

In previous studies [6, 7, 9], red light has been used to create the photoconductive effect in OET devices, most probably because a-Si is most transparent in the red. This property is particularly suitable when a-Si needs to be illuminated from the bottom. However, GaN micro-LEDs have their best performances in the violet, blue and green. Previously, 1µm to 2µm thick a-Si layers have been used in OET devices, because thinner depositions were not free from defects [6]. When we integrated the micro-LEDs with an OET device with a 1µm thickness layer of a-Si, all the light from the blue or green micro-pixels was absorbed before it reached the top a-Si surface and no effect on the particles was seen. This was due to the absorption of the a-Si being to ten times stronger at green wavelengths than in the red part of the spectrum (the absorption characteristic of a-Si shows absorption coefficient, $\alpha$, of $10^4$ $cm^{-1}$ at 625nm, and $10^5$ $cm^{-1}$ at 520nm), and even stronger absorption at blue wavelengths ($5*10^5$ $cm^{-1}$ at 450nm) [13, 14]. To overcome the higher absorption it is possible to either increase the light power or decrease the thickness of the a-Si layer. Improvement in emitted power output is possible but involves a lot of optimisation in the micro-LEDs fabrication process. We found, however, that it was possible to produce a 300nm thick a-Si layer without defects by using Plasma Enhanced Chemical Vapour Deposition (PECVD). The a-Si:H was deposited using a modified DP800 PECVD capacitively coupled system from Oxford Plasma technology with a 380mm electrode diameter and 30mm spacing. The lower grounded plate held the patterned ITO glass substrates and was heated to a temperature of 220$^o$C with the upper plate RF driven at 13.56 MHz with an input power of 10 Watts. The silicon growth rate was $0.8As^{-1}$ from pure silane at a flow rate of 75 sccm and a chamber pressure of 100mTorr. We have made the OET device with this thin, 300nm a-Si layer and, as described below, we successfully trapped and moved particles with green micro-LEDs.

3.3. Conditions for trapping

3.3.1The illumination conditions

For trapping experiments, we fixed the CMOS driver at its maximum output voltage of 4.95V. It has been shown in previous studies [11] that the I-V characteristics of micro-LEDs are size dependent. Under the same forward bias (voltage), the smaller the pixel size, the lower was the forward current. Consequently, light emitted by smaller micro-LED pixels had lower output power, as we sjhow here for the devices used (fig. 4a) and table 1). This phenomenon is due to the increase of the pixel's series resistance when their size is decreased and details of the theory explaining this phenomenon have been presented elsewhere [11]. The emitted power density measured at forward bias of 4.95V was similar for all pixels, ~ 4.5 W/cm$^2$ (details in table 1), however, this was reduced to ~ 0.4 W/cm$^2$ at the bottom surface of the sample chamber after passing through the imaging system.

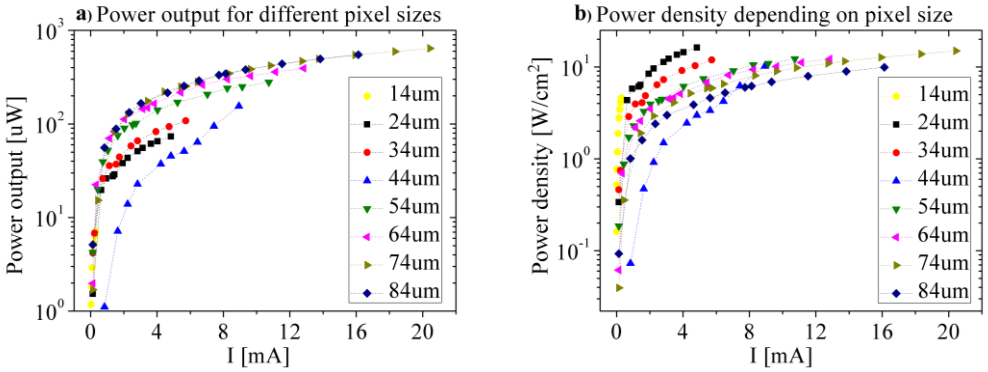


Fig.4. a) Output power as a function of current for individual green pixels as a function of diameter; b) Power density as a function of current for individual pixels of a range of diameters.

| Pixel diameter | Pixel current | Output power | Power density | Power density transmitted through the lens (9%) |
|---|---|---|---|---|
| µm | mA | µW | W/cm$^2$ | W/cm$^2$ |
| 84 | 6.0 | 255 | 4.5 | 0.4 |
| 74 | 4.4 | 231 | 5.3 | 0.5 |
| 64 | 3.3 | 144 | 4.5 | 0.4 |
| 54 | 2.4 | 96 | 4.1 | 0.4 |
| 44 | 1.7 | 73 | 4.7 | 0.4 |
| 34 | 1.5 | 40 | 4.5 | 0.4 |
| 24 | 1.0 | 26 | 5.8 | 0.5 |
| 14 | 0.6 | 11 | 7.1 | 0.6 |

Table 1. Pixel current measured during the experiment for a fixed forward bias of 4.95V; corresponding measured output power and calculated power density before and after the lens.

### 3.3.2. Particles and liquid

To achieve particle trapping, a range of parameters related to the OET device operation, such as AC drive frequency, voltage and solution conductivity, have been optimized. For trapping, we used 10µm polystyrene beads (Thermo Fisher Scientific, UK) in low concentration KCl solution and Chinese Hamster Ovary (CHO) cells in an isotonic sugar solution (0.3% Dextrose, 8.5% Sucrose in DI water). All chemicals have been supplied by Sigma Aldrich,

UK, unless otherwise stated. By using 300nm thick a-Si with green micro-LED illumination, it was found that the best conditions for trapping are: AC frequency of 10 kHz and solution conductivity of 10 $mSm^{-1}$ for 10µm polystyrene beads and 1 $mSm^{-1}$ for CHO cells.

## 4. Results and discussion

### 4.1. Trapping beads and cells: example and mechanisms

Figure 5 shows examples of polystyrene beads and CHO cells trapped by one pixel of the green micro-LED array (trapping shown in supplementary videos S1 and S2).

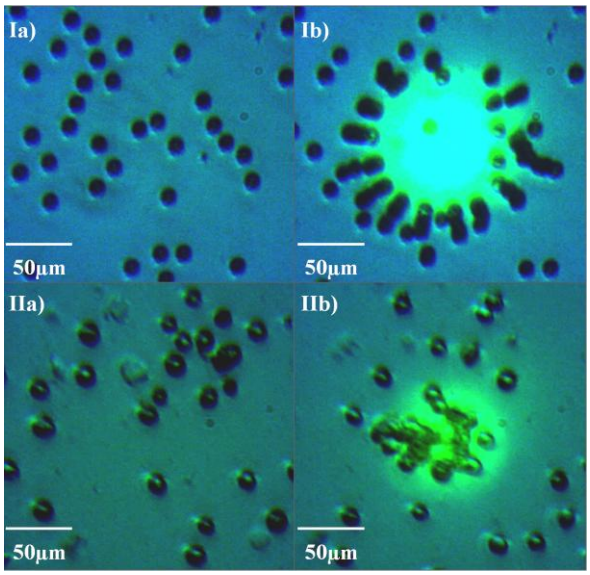


Fig. 5. Ia and IIa were taken with the LEDs turned-off; Ib and IIb were captured 40 seconds after a pixel had been turned on; Ib) Trapping beads with 74µm diameter pixel, at 20V peak to peak voltage, IIb) Trapping cells with 54µm pixel at 5V peak to peak voltage.

It was found that by operating at a relatively low frequency (10 kHz) in a low conductivity liquid (1 or 10 $mSm^{-1}$) particles could be attracted to the pixel from hundreds of microns away. Experiments were performed to study this trapping (see fig. 6).

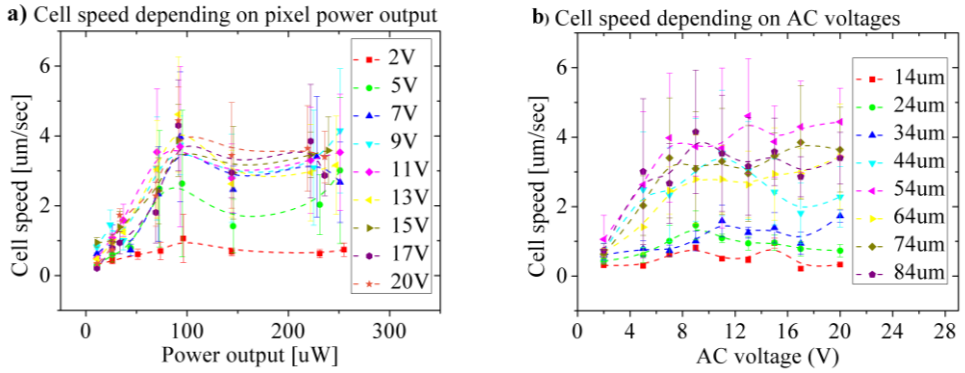


Fig. 6a) a plot of cell speed as a function of pixel power output for different AC voltages applied between ITO electrodes; b) a plot of cell speed as a function of AC voltage for different pixel sizes.

The time it took cells to move from 150µm away from the trap border to the trap center was measured and the speed calculated. This was measured as a function of the power outputed by the microLED (figure 6a) and the AC voltage applied (figure 6b)). Figure 6a) shows a linear increase in the speed of attraction from 0 to 100 µW of LED power followed by no further increase in speed. The higher output powers correspond to larger pixels, with 100 µW corresponding to a 54µm diameter pixel. Figure 6b) shows a linear increase in cell speed between 0 and 8V followed by little further increase. To better understand these trends Finite Element Method (FEM) simulations were performed.

4.2. Simulations

At these conditions two mechanisms dominate the force placed onto the particles, namely Dielectrophoresis (DEP) and Light Activated AC Electroosmosis (LACE). The DEP force is given by;

$$F = 2\pi r^3 \varepsilon_m \,\mathrm{Re}[k(\omega)]\nabla E^2$$

where $\varepsilon_m$ is the permittivity of the medium, Re[k(ω)] is the Clausius-Mossotti factor and $\nabla E^2$ is the gradient of the electrical field squared [3]. To calculate the force due to LACE the velocity of the ions (the slip velocity) in the liquid was calculated from;

$$v_{slip} = -\frac{\varepsilon_m \zeta E}{\eta}$$

Where ζ is the zeta potential, E is the electrical field and η is the viscosity. The zeta potential was calculated by determining the thickness of the charge double layer at the interface above the a-Si, thus finding its capacitance, then using circuit theory to find the potential dropped across it. Once the velocity of the liquid was known the force on the particle could be calculated by considering the force due to Stokes drag at this velocity [15]. From these equations it can be seen that DEP is proportional to the gradient of the electric filed squared and LACE is proportional to the electrical field, so in order to compare the forces these should be simulated.

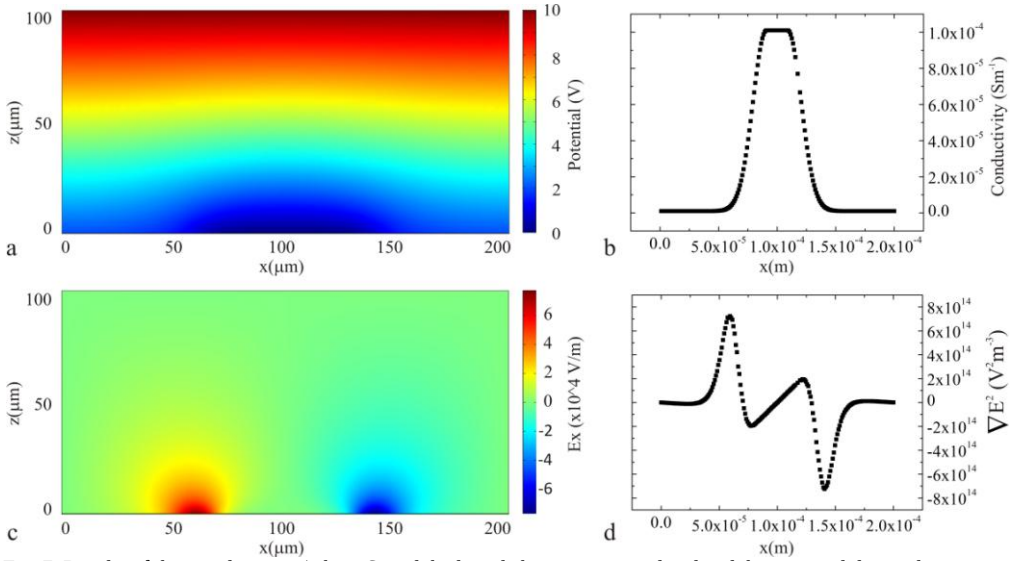


Fig. 7. Results of the simulations: a) the a-Si and the liquid above it are simulated and the potential dropped across each are shown (the a-Si is a one micron thick layer at the bottom), b) the conductivity of the a-Si as a function of

position is shown, c) the electric field in the x direction, d) the gradient of the electric field squared in the liquid just above the a-Si.

Figure 7 shows the results of simulations performed (COMSOL Multiphysics) of the a-Si and the liquid above it in the OET device. The simulations use the quasi-static approximation which in this case is valid as the device is much smaller than the wavelength of the AC field being applied. The optical intensity profiles of the four largest micro-LEDs were measured at the a-Si and were found to fit well to a profile of two Gaussian distributions with a flat top between them. It was assumed that the conductivity of the a-Si would increase linearly with the optical intensity and so conductivity profiles similar to the intensity profiles were put into the simulations (shown in fig.7b). The magnitude of the conductivity was taken at $1x10^{-6}$ $Sm^{-1}$ for the dark a-Si and $1x10^{-4}$ $Sm^{-1}$ for the illuminated a-Si (this corresponds to a light intensity of $0.5Wcm^{-2}$ [15]). This resulted in the electrical fields in the x direction shown in figure 7c) and the gradient of the electric field squared shown in figure 7d). From these simulations the forces due to DEP and LACE were calculated and are shown in figure 8.

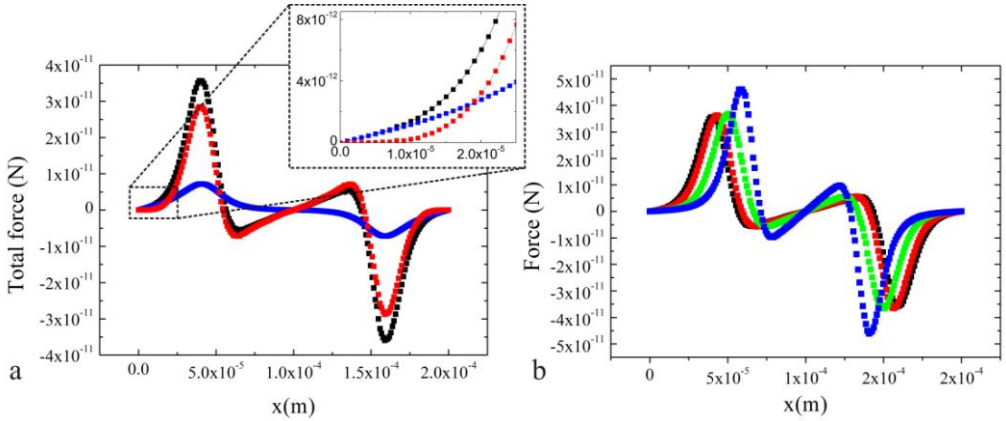


Fig. 8. a) The forces due to DEP (red), LACE (blue) and the total force (black) for the largest pixel are plotted against position, b) the total force profiles for the four largest pixels are shown.

Figure 8a) shows the force due to DEP plotted against the force due to LACE and the total force. The insert shows a blown up section of 0 to 200µm from the left showing that the LACE force dominates at a large distance from the optical spot and DEP dominates closer to the optical spot. 8b) shows that the force profiles of the traps created by the three largest pixels, 84 µm, 74 µm and 64 µm, are very similar but the fourth largest, 54µm pixel shows a higher force. The optical intensity profiles of the all four LEDs had varying widths but the Gaussian decrease in intensity at the sides of the three largest were similar. The fourth largest optical profile was sharper, and fitted a thinner Gaussian, producing this larger force. This agrees well with the results in figure 6a) where the largest micro-LEDs (corresponding to the greatest output powers) are no better at attracting the particles to the trap.

For this first demonstration of miniaturized OET controlled by CMOS-driven GaN micro-LEDs, the possible maximum power output has been limited by the current which could be driven by the CMOS chip. The CMOS could not drive voltages higher than 5V, and the 520nm micro-LEDs typical turn on voltage was 4.2V, consequently, we could not access the higher optical powers available from these micro-LEDs. The next generation CMOS driver currently being tested allows us to drive at higher voltages (up to 7V). At the same time, improvements in micro-LED fabrication will decrease the turn on voltage and improve their I-V characteristics. The next generation of CMOS driven micro-LEDs should thus emit higher optical powers form the same size LEDs thus producing higher optical intensities which should allow faster particle manipulation. Further work will also focus on creating a smaller pitch between the LEDs allowing easy movement from one pixel to the next, and on

performing time-resolved microfluorescence measurements in situ [10] for a multi-function trapping and measurement system.

## 5. Conclusion

In summary, we have demonstrated the characteristics of what we believe to be the first miniaturized OET device, by using a CMOS integrated GaN micro-LED array to generate the electrode light pattern. The trapping of polystyrene beads and cells has been achieved by switching on and off individual pixels in the array. The device was characterised by measuring the speed of cells approaching the trap and these results were compared to simulations of the forces in the device. It was found that the force increased linearly with increased output power (corresponding to larger pixels) up to 100μW but not beyond this, and this agreed well with the simulated forces. By combining this CMOS-controlled micro-LED array with smaller imaging system, this technology has the potential to create scalable, portable and low-cost micromanipulation devices.

## Acknowledgements

**This work was funded under the Scottish Consortium on Integrated Microphotonic Systems and by EPSRC. SLN thanks the Royal Academy of Engineering for support under a personal research fellowship**